Noncommutative band offset at α-Cr_2O_3/α-Fe_2O_3(0001) heterojunctions

S. A. Chambers, Y. Liang, and Y. Gao
Environmental Molecular Sciences Laboratory, Pacific Northwest National Laboratory, Richland, Washington 99352
(Received 4 November 1999)

We have measured the valence-band discontinuity at artificially structured, epitaxial heterojunctions of α-Cr_2O_3(0001) and α-Fe_2O_3(0001). Layered film structures of these two materials maintain the in-plane lattice parameter of α-Fe_2O_3(0001). Thus the α-Cr_2O_3(0001) layers are under a 2.4% tensile stress. A partial inward relaxation in α-Cr_2O_3(0001) layers along the c axis is also observed, revealing the presence of artifically structured epilayers with a c/a ratio of 2.70, compared to 2.78 in bulk α-Cr_2O_3(0001). The valence-band offsets are -0.3 ± 0.1 and $+0.7\pm0.1$ eV when the top layer is Fe_2O_3 and Cr_2O_3, respectively. The noncommutativity in the band offset is not due to either anisotropic strain or quantum confinement, but rather appears to be due to a growth-sequence-dependent interface dipole.

I. INTRODUCTION

III–V and II–VI semiconductor heterojunctions have proven to be useful material systems in a wide range of solid-state electronic and optoelectronic devices. In such devices, the valence- and conduction-band discontinuities, or band offsets, at interfaces of dissimilar semiconductors are important parameters in determining such properties as electron-hole pair separation and confinement, leakage current, and gate voltage swing.[1] In comparison, much less is known about analogous interfacial systems involving epitaxial oxide materials. Nevertheless, recent developments point to the importance and potential unique applications afforded by the use of oxides. For instance, epitaxial oxide films have been used as ferroelectric gates in field-effect transistors.[2] In addition, the magnetic properties of certain transition-metal oxides have given rise to classes of magnetic devices involving spin-polarized electron transport.[3] As in the case of traditional compound semiconductors, successful device fabrication and operation depend critically on gaining an in-depth understanding of oxide thin-film and interfacial properties. Critical scientific issues range from adhesion of dissimilar oxide materials to interface electronic structure and its effect on electron transport and scattering. A key aspect of interfacial electronic structure that needs to be understood for epitaxial oxides, but for which we have virtually no experimental results, is the band offset at oxide/oxide heterojunctions.

In this paper, we describe a successful synthesis and band-offset determination for epitaxial α-Fe_2O_3/α-Cr_2O_3(0001) superlattices, and we point out unusual, but potentially useful, band-offset behavior. These structures were grown by oxygen-plasma-assisted molecular-beam epitaxy (OPA-MBE) on α-Al_2O_3(0001) substrates.[4] Valence-band offsets were measured by core-level x-ray photoemission using a method pioneered by Kraut *et al.*[5] In summary, we have found that once an α-Fe_2O_3(0001) epitaxial layer of thickness equal to a few hundred Å or more has been grown, all subsequent α-Cr_2O_3(0001) layers remain under lateral tension and exhibit the same in-plane lattice parameter as α-Fe_2O_3(0001). The out-of-plane lattice parameter contracts slightly to offset the in-plane strain. Thus all heterojunctions formed in this way consist of unstrained α-Fe_2O_3(0001) and artifically-strained α-Cr_2O_3(0001). In addition, there is a significant noncommutativity in the band offset. This feature may make superlattices of these materials useful for effective spatial separation of electrons and holes due to the potential gradient that is expected to develop over a few periods of the superlattice.

II. EXPERIMENT

The system used to conduct this work is described in detail elsewhere.[4] In brief, the system consists of three coupled UHV chambers that perform OPA-MBE, atomic force microscopy, (AFM), scanning tunneling microscopy, (STM), and x-ray photoelectron spectroscopy (XPS) diffraction (XPD). Specimens are readily transferred between these chambers, and the loadlock under UHV conditions by means of a transfer tube.

Substrates of α-Al_2O_3(0001) were initially cleaned by ultrasonic washing in acetone and isoproposal prior to insertion into UHV. They were then further cleaned in the MBE chamber by exposure to an oxygen plasma beam at a chamber pressure of 2×10^{-5} torr and a plasma power level of 250 W, with the sample at room temperature. All epitaxial films were grown at a substrate temperature of $\sim$500 °C using a metal evaporation rate of $\sim$0.1 Å/sec, an oxygen partial pressure of 2×10^{-5} torr, and an electron cyclotron resonance plasma power level of 250 W.

The in-plane lattice parameters and (00) beam intensities of the growing film surfaces were monitored in real time using reflection high-energy electron diffraction (RHEED) in the MBE chamber. Following cooldown and RHEED measurements made with the film surfaces near room temperature, the specimens were transferred to the photoemission chamber for core- and valence-level XPS using monochromatic Al $K\alpha$ x rays. An electron flood gun was required for all photoemission measurements due to the insulating nature of these materials. All deep core-level spectra were shifted so the O 1s peak fell at 530.0 eV. Likewise, all shallow core-level and valence-band spectra were shifted to place the O 2s peak at 23.0 eV. However, these choices are arbitrary, and did not affect the subsequent analysis in any way, since the

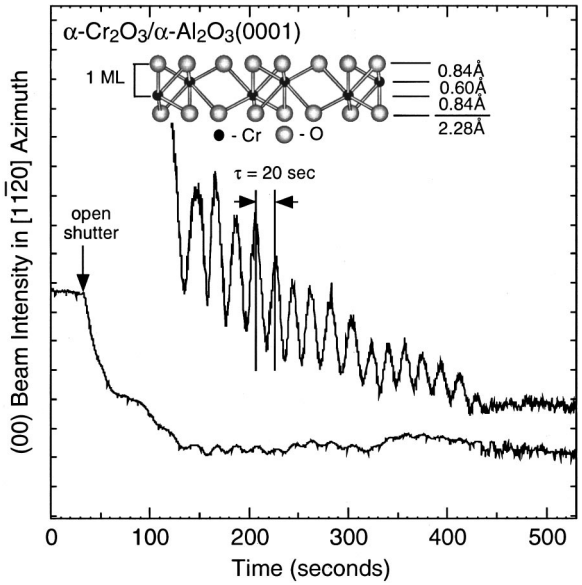

FIG. 1. RHEED (00) beam intensity oscillations during the OPA-MBE growth of α-Cr_2O_3 on α-Al_2O_3(0001). The 30-keV beam was aligned parallel to [11$\bar{2}$0]. The nominal metal evaporation rate, as measured by a QCO adjacent to the substrate, was ~0.1 Å/sec.

band-offset determination depends on binding energy differences rather than absolute values.[5]

The thicknesses of α-Fe_2O_3 films were determined by Rutherford backscattering (RBS) conducted *ex situ* in a dedicated RBS chamber.[6] Thicknesses for α-Cr_2O_3 films were determined by RHEED intensity oscillations, as discussed below. The total film thickness of α-Cr_2O_3/α-Fe_2O_3 superlattice structures determined absolutely by TEM were in agreement with those estimated from RBS and RHEED oscillations to within ~10–12 %. A JEOL 2010 microscope was used for all TEM measurements.

III. RESULTS

A. Film and interface structure

The in-plane lattice parameters (a) for bulk α-Al_2O_3(0001), α-Cr_2O_3(0001) and α-Fe_2O_3(0001) are 4.76, 4.92, and 5.03 Å, respectively. The associated out-of-plane lattice parameters (c) are 12.99, 13.7, and 13.7 Å, respectively. All three materials exhibit a corundumlike crystal structure. The in-plane lattice mismatch, defined as $(a_{film} - a_{sub})/a_{sub}$, is +3.36 and +5.80% for α-Cr_2O_3 and α-Fe_2O_3 on α-Al_2O_3(0001), respectively. Previous work has shown that the large lattice mismatch for α-Fe_2O_3 on α-Al_2O_3(0001) results in three-dimensional island growth under the best of conditions.[7,8] The resulting epitaxial nanocrystals uniformly orient in the same way on the substrate, and eventually agglomerate after several hundred to ~1000 Å. In contrast, there is to the best of our knowledge nothing in the literature about the OPA-MBE growth of α-Cr_2O_3 on α-Al_2O_3(0001). The smaller lattice mismatch improves prospects for a more laminar growth mode.

In Fig. 1 we show a typical (00) beam RHEED intensity vs time curve for α-Cr_2O_3 growth on α-Al_2O_3(0001) with the primary beam aligned parallel to [1120]. Nearly identical

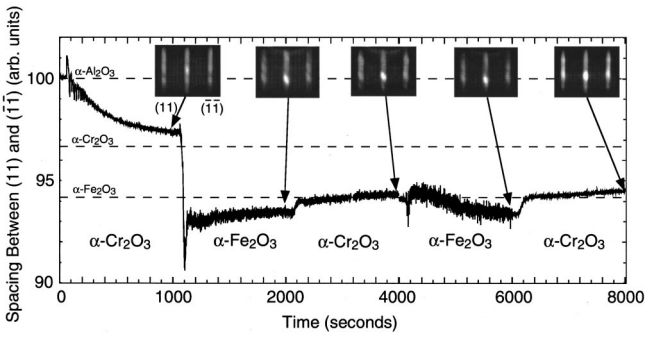

FIG. 2. RHEED streak spacing during α-Cr_2O_3/α-Fe_2O_3 superlattice growth on α-Al_2O_3(0001). The 30-keV beam was aligned parallel to [1$\bar{1}$00]. The metal evaporation rate was ~0.1 Å/sec, as measured by a QCO adjacent to the substrate.

oscillations were measured when the primary beam was aligned along [11 00]. The Cr shutter was opened at $t = 35$ sec. The intensity dropped monotonically during the first ~40 sec of growth, and then exhibited weak, nonperiodic oscillations for the next ~60 sec. The intensity then underwent weak, periodic oscillations for the next ~310 sec that gradually damped to zero amplitude. This behavior suggests that nominal layer-by-layer growth occurred during the periodic oscillatory portion, from 135 to 445 sec. The period was ~20 sec during this portion of the growth, yielding ~20 sec as the characteristic time for the completion of full monolayers of α-Cr_2O_3 in the corundum structure.[9] Thus ~16 complete monolayers grew in a quasi-layer-by-layer fashion. However, the beam intensity at all times during these oscillations remained well below that of the starting substrate, indicating that the film surface has a much higher step density than the substrate surface. The in-plane lattice parameter steadily increased from the value of the substrate to that of α-Cr_2O_3 throughout the growth, as seen in Fig. 2. Here we plot the streak spacing in pixels between the (11) and 1 1) RHEED beams, normalized to a value of 100 for α-Al_2O_3(0001), for several layers of α-Cr_2O_3 and α-Fe_2O_3 in a superlattice structure. The primary beam was aligned along [1$\bar{1}$00]. The streak spacings expected for bulk α-Cr_2O_3 and α-Fe_2O_3 are shown as dashed lines, as is that for the substrate. The cessation of RHEED oscillations after 16 ML may signal a transition from layer-by-layer to step-flow growth. Inspection of Fig. 2 reveals that the first α-Cr_2O_3 film is still in the process of relaxing when the intensity oscillations cease.

The brief oscillatory period shown in Fig. 1 allows the Cr_2O_3 growth rate to be calibrated at ~0.050 ML/sec, which is equivalent to a α-Cr_2O_3(0001) growth rate of ~0.12 Å/sec. Here 1 ML of α-Cr_2O_5(0001) is defined as two layers of Cr, and one close-packed O layer in the corundum structure. Each Cr layer has one-third the number of atoms found in the close-packed O layer. This basic structural ML unit is shown in Fig. 1. Since the growth is carried out under oxygen-rich conditions, the growth rate is determined by the rate at which Cr cations are delivered to the substrate. The number density of Cr cations in the α-Cr_2O_5(0001) structure is such that 1.0 Å of Cr metal will result in 1.01 ML of α-Cr_2O_3(0001), which will add 2.3 Å of film thickness. Based on the period of the RHEED oscillations shown in

Fig. 1, the thickness of the first α-Cr_2O_3 film is estimated to be 120 Å. No sustained RHEED intensity oscillations were observed during α-Fe_2O_3 film growth at any time, as is the case for α-Fe_2O_3 grown directly on α-$Al_2O_3(0001)$.[7,8]

Returning now to Fig. 2, a RHEED pattern of the zeroth-order Laue zone obtained after closing the Cr shutter, but before opening the Fe shutter, after the completion of the first α-Cr_2O_3 film, is shown in Fig. 2. The streaky character, which was observed throughout the growth, indicates that the film surface is reasonably flat. The in-plane lattice parameter had not yet fully converged to the value of bulk α-Cr_2O_3, although it was quite close by the end of the growth. Following a very large apparent increase ($\sim$7%) at the onset, the in-plane lattice parameter rapidly converged to a value very close to that of bulk α-Fe_2O_3 upon opening the Fe shutter and initiating the first α-Fe_2O_3 layer growth. The apparent increase in lattice parameter to a value well above that of α-Fe_2O_3 has been seen before for growth directly on α-$Al_2O_3(0001)$, and has been ascribed to the formation of a highly strained, buckled wetting layer that forms in response to the 5.8% lattice mismatch.[7,8] Presumably, a similar phenomenon occurs here. The RHEED pattern taken at completion of the first α-Fe_2O_3 film reveals that the surface remains reasonably smooth, although some transmission is evident based on the intensity modulation along the streaks, betraying some roughening at the film surface. The thickness of each α-Fe_2O_3 layer was determined to be $\sim$140 Å based on a calibration of the QCO growth rate with RBS measurements for pure α-$Fe_2O_3(0001)$ films grown on α-$Al_2O_5(0001)$ substrates.

Very curious behavior of the in-plane lattice parameter was then observed upon growth of the second α-Cr_2O_3 layer, which was the *first* one to be grown on α-Fe_2O_3. The α-Cr_2O_3 lattice parameter remained fixed at the value expected for bulk α-Fe_2O_3. Thus the α-Cr_2O_3 layer was found to be in lateral tension on α-Fe_2O_3. This behavior was also observed after the completion of all other α-Cr_2O_3 layers in several superlattice structures, including some that were up to 600 Å thick. In addition, the same result was obtained from RHEED patterns for superlattice structures in which the specimen was allowed to cool to near room temperature after the completion of each layer. A series of such streak spacing measurements is shown in Fig. 3. These are more accurate than those obtained when the specimen was hot and the Cr and Fe electron-beam evaporators were running because of electromagnetic interference (EMI) between the various filaments and the RHEED beam. Such EMI causes slight distortions in the patterns, as can be seen by inspection of Fig. 2, producing inaccuracies in the measured streak spacings. These inaccuracies may explain, for instance, why the apparent in-plane lattice parameters of α-Fe_2O_3 films shown in Fig. 2 deviate slightly from that of bulk α-Fe_2O_3. However, no such deviations were seen when the sample was cool. As seen in Fig. 3, the streak spacing for thick and thin films of both α-Fe_2O_3 and α-Cr_2O_3 are quantitatively equal, and the value is $5.9\pm0.3\%$ smaller than that of α-$Al_2O_3(0001)$. This value is within experimental error of the in-plane lattice mismatch between α-$Fe_2O_3(0001)$ and α-$Al_2O_3(0001)$, indicating that Fe_2O_3 films are relaxed, whereas those of Cr_2O_3 are pseudomorphic on the Fe_2O_3 lattice, even for α-Cr_2O_3 film

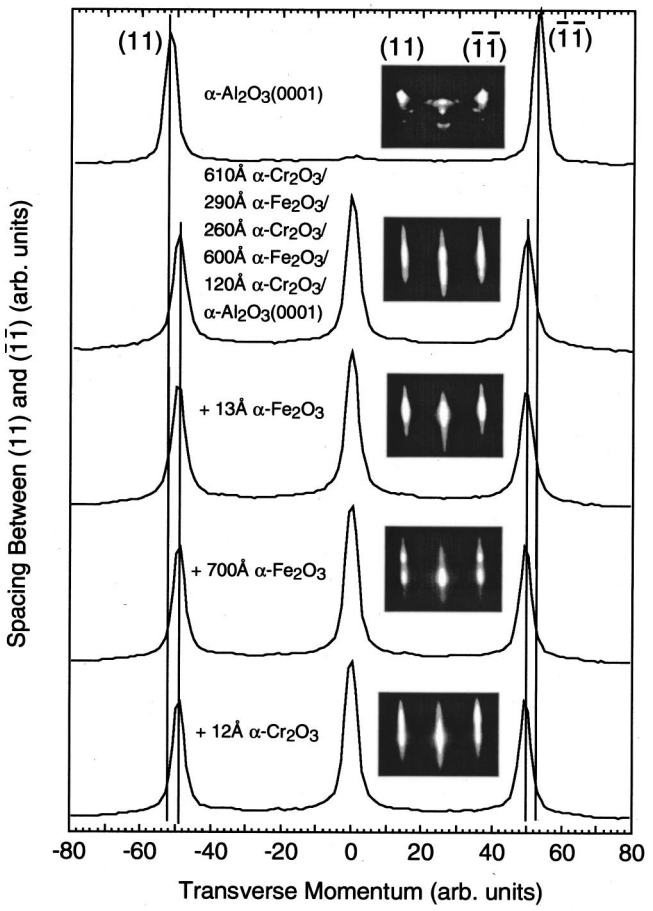

FIG. 3. RHEED patterns and transverse line scans, with the 30-keV primary beam aligned along $[1\bar{1}00]$, for an α-$Al_2O_3(0001)$ substrate, and for thick and thin epitaxial films of α-$Fe_2O_3(0001)$ and α-$Cr_2O_3(0001)$.

thicknesses of several hundred Å. This surprising result may be related to the fact that the out-of-plane lattice parameter *c* may contract in order to compensate for the in-plane tensile strain. In order to test this hypothesis, we turn to TEM and related selected-area diffraction patterns, which are shown in Figs. 4 and 5.

Figures 4(a) and 4(b) show low- and high-resolution bright-field TEM micrographs of a superlattice structure obtained in cross section. The nominal layer thicknesses, obtained by *ex situ* RBS and RHEED oscillations for Fe_2O_3 and Cr_2O_3 layers, respectively, were 740-Å α-Cr_2O_3/140-Å α-Fe_2O_3/120-Å α-Cr_2O_3/140-Å α-Fe_2O_3/120-Å α-Cr_2O_3/α-$Al_2O_3(0001)$. The total thickness nominal thickness, 1260 Å, is in reasonable agreement with the thickness measured directly by TEM, 1450 Å. The individual interface locations cannot be unambiguously determined, with the exception of those at the bottom (α-Cr_2O_3/α-Al_2O_3) and top (epoxy/α-Cr_2O_3) of the stack. The approximate locations are indicated with lines in Fig. 4(a). However, it is clear from the low-resolution image that the dislocation density is high in the first α-Cr_2O_3 layer. The high-resolution lattice image shown in Fig. 4(b) reveals an individual misfit dislocation. The high dislocation density in the first α-Cr_2O_3 layer is presumably due to the large lattice mismatch between α-Cr_2O_3 and α-Al_2O_3. In Fig. 5 we show a selected area diffraction pattern obtained for the entire film stack and a

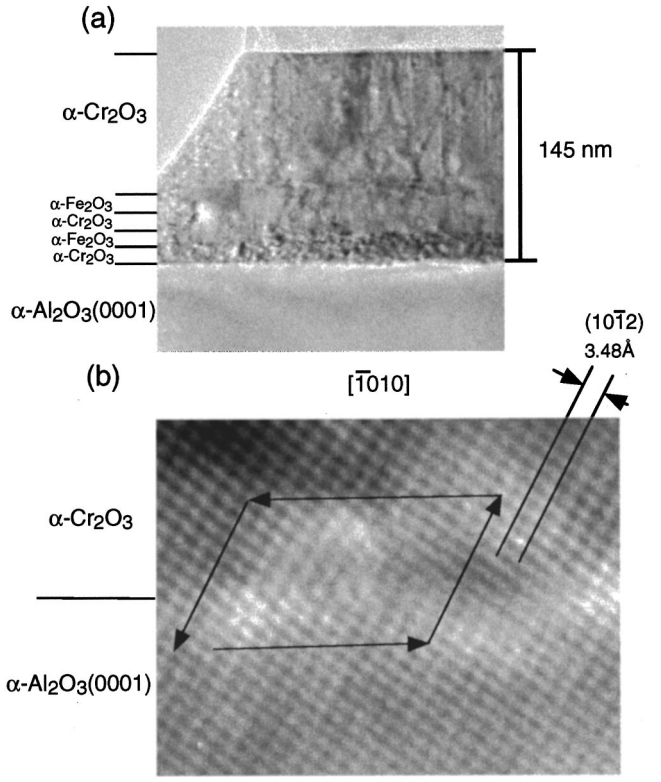

FIG. 4. (a) Low-resolution and (b) high-resolution bright-field TEM micrographs of a α-Cr_2O_3/α-Fe_2O_3 superlattice grown on α-$Al_2O_3(0001)$. The 200-keV beam was aligned parallel to $[10\bar{1}0]$.

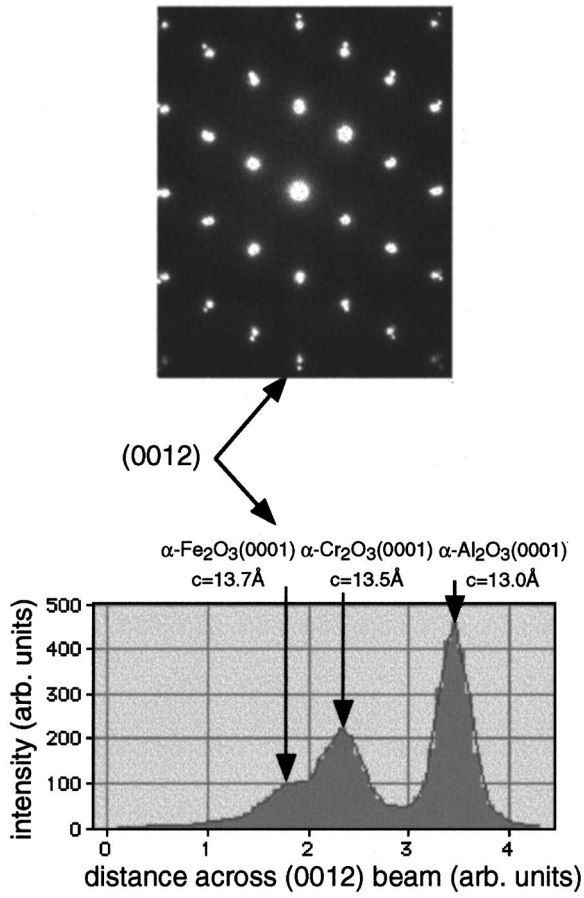

FIG. 5. TEM-selected area diffraction pattern for the α-Cr_2O_3/α-Fe_2O_3 superlattice grown on α-$Al_2O_3(0001)$, described in conjunction with Fig. 4, along with an intensity profile along the (0012) diffraction beam.

portion of the substrate. The crystal orientation was the same as that shown in Fig. 4. Examination of the less intense diffraction beams reveals the presence of three individual beams distributed along the growth direction. A line scan across the (0012) beam is shown at the bottom of Fig. 5. The largest peak is the (0012) reflection from the substrate, for which c is 13.0 Å. Likewise, (0012) reflections are also seen corresponding to the relaxed Fe_2O_3 layers and the distorted Cr_2O_3 layers. The peak positions reveal that the strained Cr_2O_3 layers possess a c value of 13.5 Å. Thus these layers relax inwardly by ~0.2 Å in the c direction in order to partially compensate for the tensile stress created by remaining pseudomorphic on Fe_2O_3.

In Fig. 6 we show Fe $2p$, Cr $2p$, and O $1s$ core-level spectra obtained for thick (several hundred Å) films of Fe_2O_3 (a) and Cr_2O_3 (b), and an ~12-Å-thick film of Cr_2O_3 on Fe_2O_3 (c). Spectra for a thin film of Fe_2O_3 on Cr_2O_3 are not shown, because these spectra are the same as those shown in Fig. 6(c). The spectra for the thin film, which probe the interfacial region, are the same as those for the thick films, which are representative of the pure materials. The Fe and Cr $2p$ spectra are strongly affected by shake-up, phonon broadening, and multiplet splitting in the final state.[10] Such well-resolved spectra are useful fingerprints of the local electronic and magnetic environment of the Fe(III) and Cr(III) cations in the oxide lattice. The fact that the thin-film spectra are the same as those of the pure materials reveals that there is no detectable reduction of either Fe or Cr at the interface, indicating no oxygen vacancies. In addition, the O $1s$ line shapes and peak widths are virtually indistinguishable for the three specimens, indicating that the oxygen sublattice is unperturbed across the interface. Extensive intermixing, leading to substrate atom outdiffusion to the free surface measurable by XPS does not occur with these materials. Cr (Fe) was never detected by XPS in the near-surface region of Fe_2O_3 (Cr_2O_3) films of any thickness great enough to completely attenuate photoemission form the underlying layer. Nevertheless, limited intermixing at individual interfaces probably does occur, since α-Fe_2O_3 and α-Cr_2O_3 form a solid solution over the complete range of composition.[11] Indeed, some Fe was detected by secondary ion mass spectrometry at the surface of a terminal 120-Å-thick layer of α-Cr_2O_3, indicating limited Fe outdiffusion. However, Cr (Fe) $2p$ intensity attenuation upon growth of Fe_2O_3 (Cr_2O_3) thin films is consistent with reasonably abrupt interfaces.

B. Band-offset determination

In Fig. 7 we show the shallow Fe and Cr $3p$ core levels, along with the valence bands, from which the band offsets were determined. Determining the core-level binding energies in a consistent and reproducible way was made somewhat difficult by multiplet splitting, which complicates the line shape. Nevertheless, taking the difference between these core-level binding energies and the leading edge of the valence bands, as shown in the inset, for surfaces of the pure materials leads to values of $\Delta E_{\mathrm{Me}\,3p-\mathrm{VB}}$ of 42.62 ± 0.03 and

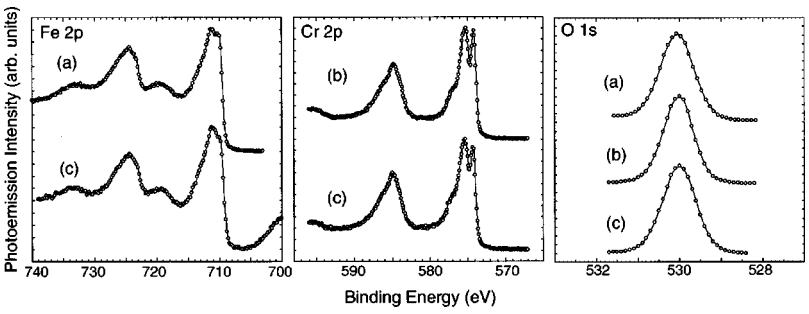

FIG. 6. Fe $2p$, Cr $2p$, and O $1s$ core-level photoemission spectra obtained at normal emission for (a) unstrained α-Fe_2O_3(0001), (b) strained α-Cr_2O_3(0001), and, (c) $a\sim$12-Å-thick film of α-Cr_2O_3(0001) on α-Fe_2O_3(0001).

54.26 ± 0.09 eV for α-Cr_2O_3(0001) and α-Fe_2O_3(0001), respectively. Likewise, differences in core-level binding energies, $\Delta E_{\mathrm{Fe}\,3p-\mathrm{Cr}\,3p}$, for the thin films were 11.99 ± 0.09 and 12.34 ± 0.08 eV for Fe_2O_3 on Cr_2O_3 and Cr_2O_3 on Fe_2O_3, respectively. Each of these numbers is the average value from four separate film growths, and the uncertainties are standard deviations. The valence-band offsets are then determined to be -0.3 ± 0.1 and $+0.7\pm0.1$ eV for Fe_2O_3 on Cr_2O_3 and Cr_2O_3 on Fe_2O_3, respectively. Here our sign convention is that the band offset is negative (positive) if the overlayer band is bound more strongly (weakly) than the underlayer band. We emphasize that the strain configuration is unchanged as a result of inverting the growth sequence; the α-Cr_2O_3 layers are under a 2.4% tensile stress, whereas the α-Fe_2O_3 layers are relaxed, as discussed in Sec. III A. Therefore, strain is not a factor in the observed band-offset noncommutativity. In fact, the valence-band offset at the *first* α-Fe_2O_3/α-Cr_2O_3 interface grown on a given α-Al_2O_3(0001) substrate, for which both layers are relaxed (see the left side of Fig. 2), is also -0.3 ± 0.1 eV, revealing that strain apparently does not affect the band offset for this oxide/oxide heterojunction in any measurable way.

The band offsets are shown in an energy-level diagram in Fig. 8(a). Here we have neglected band bending, which is likely to be negligible compared to the film thicknesses used because the films are undoped. Using the bulk band gaps of Fe_2O_3[12] and Cr_2O_3,[13] we can also estimate the conduction-band offsets, as shown in Fig. 8(a). It is likely that the band gap of strained, epitaxial α-Cr_2O_3(0001) differs from that of the unstrained bulk material. In order to determine if such a difference exists, we attempted to measure the band gap of

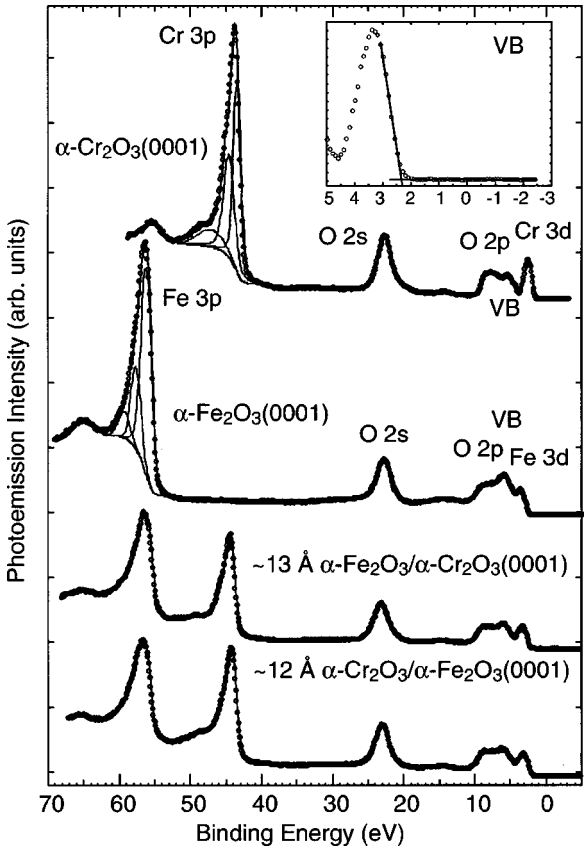

FIG. 7. Fe $3p$, Cr $3p$, O $2s$, and valence band (VB) spectra for strained α-Cr_2O_3(0001), unstrained α-Fe_2O_3(0001), and α-Fe_2O_3(0001)/α-Cr_2O_3(0001) and α-Cr_2O_3(0001)/α-Fe_2O_3(0001) heterojunctions.

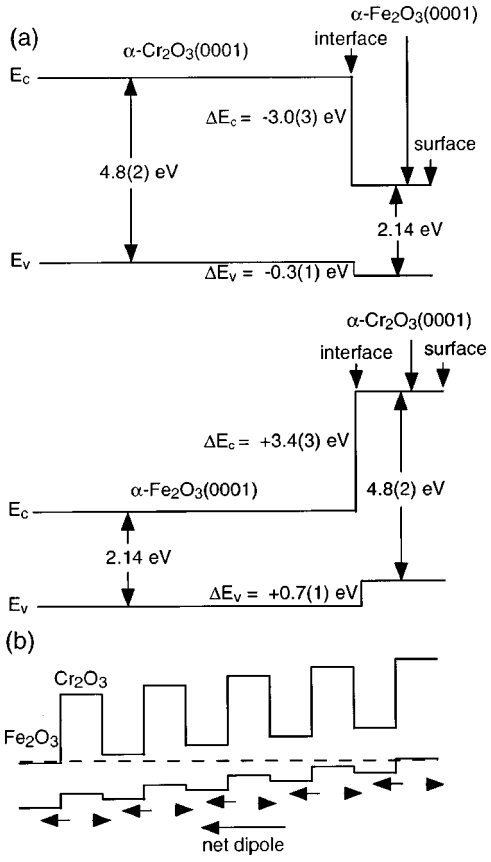

FIG. 8. Energy-level diagrams showing (a) the noncommutative band offsets for α-Fe_2O_3(0001)/α-Cr_2O_3(0001) and α-Cr_2O_3(0001)/α-Fe_2O_3(0001) heterojunctions, and (b) the potential gradient that develops over several superlattice periods as a result of the noncommutative band offsets.

epitaxial α-Cr_2O_3/α-$Fe_2O_3/\cdots/\alpha$-$Al_2O_3(0001)$ by high-resolution electron-energy-loss spectroscopy. However, the energy-loss region within the Cr_2O_3 band gap contained features created by excitation of surface states, and an unambiguous determination of the band gap was not possible. Therefore, we have used the band gap of bulk Cr_2O_3 in Fig. 8(a).

IV. DISCUSSION

Based on what is known about traditional semiconductor band offsets, there are three possible physical causes for the noncommutative band offset seen here. The first of these is strain. Strain is known to have a large effect on some semiconductor band offsets. One example is Si/Ge. The lattice parameters of Si and Ge differ by 4%, and the critical thickness of epitaxial films of one on a substrate of the other is only a few monolayers. The valence-band offset of thin, pseudomorphic Si on Ge(001) is 0.74 eV whereas that for thin, pseudomorphic Ge on Si(001) is 0.17 eV.[14] However, in this case, the strain configuration is different for the two interfaces; the thin epitaxial layer of Ge (Si) is in compression (tension) and the Si (Ge) substrate is unstrained. In contrast, $Cr_2O_3(Fe_2O_3)$ is under tension (unstrained) for both Fe_2O_3/Cr_2O_3 and Cr_2O_3/Fe_2O_3 heterojunctions. In addition, band-offset measurements for Fe_2O_3/Cr_2O_3 heterojunctions in which both layers are relaxed are numerically the same as those for which the Cr_2O_3 layer in under tension and the Fe_2O_3 layer is relaxed. Therefore, we rule out strain as having any significant effect on the band offsets in this materials system

The second possible cause is quantum confinement. Limiting the thickness of an epitaxial layer can have the effect of altering the energy eigenvalues within the valence and conduction bands, thereby changing the band offsets.[15] The change in eigenvalues depends on layer thickness. To test this possibility, we grew Fe_2O_3 and Cr_2O_3 overlayers of different thicknesses to see if the band offsets varied with thickness, and they did not. Therefore, quantum confinement is not a factor.

The third possible cause is a difference in interface dipole due to variations in the atomic configuration on either side of the interface. It has been shown that in theory, the exact atomic configuration at the interface can have a nonnegligable effect on band offsets at Ge/GaAs and ZnSe/GaAs heterojunctions.[1] In addition, noncommutative band-offset behavior has been observed for lattice-matched $Ga_{0.47}In_{0.53}As/InP(001)$, and was ascribed to the same cause.[16] Fe is slightly more electronegative than Cr. Therefore, a dipole exists at each heterojunction interface, even if the interface is structurally perfect and completely abrupt. The dipole at a Fe_2O_3/Cr_2O_3 interface will be equal but opposite to that at a Cr_2O_3/Fe_2O_3 interface if there is no intermixing, or if the extent of intermixing is the same for the two interfaces, as illustrated in Fig. 9. Here, we show a thin epitaxial layer of Cr_2O_3 sandwiched between two layers of Fe_2O_3, and the associated interfaces, which are depicted as being perfectly abrupt on an atomic scale. The interface dipole moments are equal in magnitude but opposite in direction, as shown in Fig. 9. The dipoles will change in magnitude but in the same way, leading to a net cancellation, if

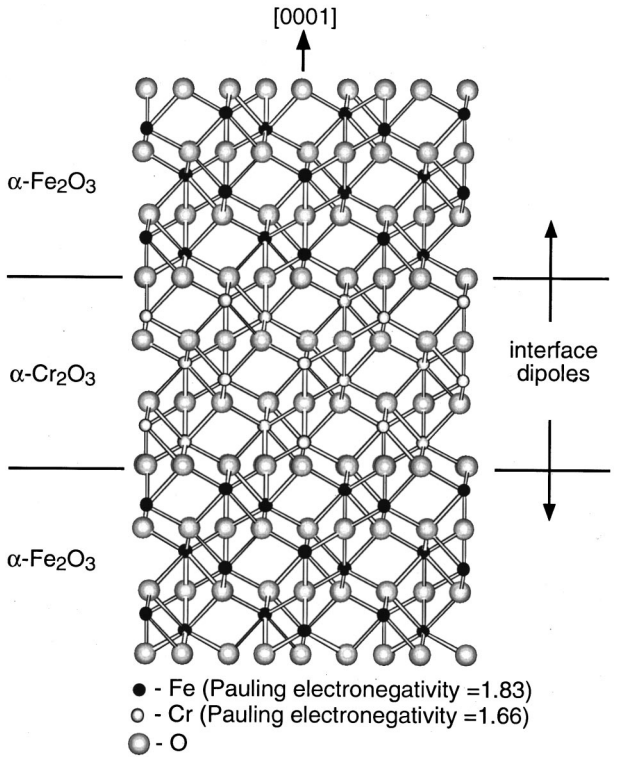

FIG. 9. Schematic structural diagram of an atomically abrupt α-Fe_2O_3/α-Cr_2O_3/α-$Fe_2O_3(0001)$ layered system, showing the equal but opposite dipole moments that develop at each interface due to the different electronegativities of Cr and Fe.

intermixing occurs to the same extent at each interface. However, a nonzero net dipole will be established for each full period of the superlattice if the extents of intermixing are different at the two interfaces. This effect is shown schematically in Fig. 8(b). Detecting slight differences in intermixing between the two interfaces is exceedingly difficult. Nevertheless, we are currently designing experiments to do so. One technique that may yield definitive answers is TEM lattice imaging based on inelastically scattered electrons that have excited core-level transitions in Cr and Fe.[17] By setting the energy-loss spectrometer at an energy window covering the *K* edge of Cr with a Gatan energy filter system, regions of the interfacial region that are rich in Cr will be highlighted. Likewise, for Fe, when the energy window covers the Fe *K*-edge loss feature. Accordingly, with a spatial resolution of $\sim$1 nm, this measurement may allow the extent of intermixing to be determined on each side of the two interfaces. Another technique that may be useful is multi-atom resonant photoemission (MARPE).[18] Interatomic resonant photoemission involving Fe and Cr might allow the extent of interfacial intermixing to be determined for specimens consisting of thin films of Cr_2O_3 on Fe_2O_3. Measuring the resonant enhancement of Cr $2p$ photoemission as the Fe $2p$-$3d$ transition is excited should in principle yield information on the spatial distribution outdiffused Fe in the Cr_2O_3 layer. The characteristic maximum sensing length of MARPE has been determined to be $\sim$20 Å in Fe/Cr metallic alloys.[19] Comparison of MARPE spectra of Cr_2O_3/Fe_2O_3 interfaces with those of well-defined $Cr_xFe_{2-x}O_3$ reference films should allow the extent of outdiffusion of Fe into Cr_2O_3 to be determined.

A significant implication of the noncommutative band-

offset behavior noted above is that a potential gradient accompanying the net dipole would be established in superlattices of these materials. This situation is depicted schematically in Fig. 8(b). The potential gradient would ultimately be self-limiting over approximately five superlattice periods as the valence-band maximum at one end of the superlattice structure becomes higher in energy than the conduction-band minimum at the other end. At this point, carriers would flow and establish a gradient in the direction opposite to that created by the noncommutative band offsets. However, photoexcitation of electron-hole pairs anywhere in the structure would result in two kinds of carrier separation. First, the type-II band offset that exists would naturally drive electrons and holes to opposite ends of the structure. Second, the gradient that develops over several superlattice periods would drive electrons (holes) toward the low-(high-) electron-energy end of the structure. The efficiency with which this process occurs would depend on electron and hole mobilities and layer thicknesses, particularly for the Cr_2O_3 layers, at which the larger of the two potential barriers exists. Unfortunately, the insulating nature of these materials made it necessary to use an electron flood gun to neutralize the photoemission-induced surface charge, so it was not possible to track the absolute position of the core levels and, therefore, the valence-band maximum relative to the Fermi level, as different periods of the superlattices were grown. However, experiments are planned in which thin epitaxial films of Cr_2O_3 and Fe_2O_3 will be grown on Pt(111) so the valence-band energy relative to an absolute Fermi level can be tracked over at least a few superlattice periods. The in-plane lattice parameter of Pt(111) is the same as that of α-Al_2O_3(0001), and high-quality films of Pt have been grown by MBE on α-Al_2O_3(0001).[20]

V. CONCLUSIONS

In summary, MBE-grown α-Fe_2O_3(0001)/α-Cr_2O_3(0001) superlattices, in which the Cr_2O_3 layers are in lateral tension by $\sim$2% and the Fe_2O_3 layers are unstrained, exhibit unusual noncommutative band-offset behavior. This noncommutativity is in all likelihood caused by a growth-order-dependent interface dipole. Furthermore, the noncommutativity produces a potential gradient over several periods of the sueprlattice that may be useful for enhanced effectiveness in spatially separating electrons and holes.

ACKNOWLEDGMENTS

This work was supported in part by PNNL Laboratory Directed Research and Development funds, and in part by the U.S. Department of Energy, Office of Science, Office of Basic Energy Sciences, Division of Materials Science. The work was performed in the Environmental Molecular Sciences Laboratory, a national scientific user facility sponsored by the Department of Energy's Office of Biological and Environmental Research and located at Pacific Northwest National Laboratory. The authors are grateful to M. A. Henderson for performing high-resolution electron-energy-loss and secondary-ion-mass spectroscopy measurements on the α-Cr_2O_3(0001) surface.

[1] For an excellent review of semiconductor heterojunction band offsets, see A. Francioso and C. G. Van de Walle, Surf. Sci. Rep. **25**, 1 (1996).
[2] S. Mathews, R. Ramesh, T. Venkatesan, and J. Benedetto, Science **276**, 238 (1997).
[3] G. A. Prinz, Phys. Today **48**, 58 (1995).
[4] S. A. Chambers, Surf. Sci. Rep. (to be published).
[5] E. A. Kraut, R. W. Grant, J. R. Waldrop, and S. P. Kowalczyk, Phys. Rev. Lett. **44**, 1620 (1980); Phys. Rev. B **28**, 1965 (1983).
[6] S. Thevuthasan, C. H. F. Peden, M. H. Engelhard, D. R. Baer, G. S. Herman, W. Jiang, Y. Liang, and W. J. Weber, Nucl. Instrum. Methods Phys. Res. A **420**, 81 (1999).
[7] S. I. Yi, Y. Liang, and S. A. Chambers, J. Vac. Sci. Technol. A **17**, 1737 (1999).
[8] S. I. Yi, Y. Liang, S. Thevuthasan, and S. A. Chambers, Surf. Sci. **443**, 212 (1999).
[9] B. A. Joyce, J. Cryst. Growth **99**, 9 (1990).
[10] M. S. McIntyre and D. G. Zetaruk, Anal. Chem. **49**, 1521 (1977).
[11] A. Muan A. and S. Somiya, J. Am. Ceram. Soc. **207**, 4 (1960).
[12] S. Mohanty and J. Ghose, J. Phys. Chem. Solids **53**, 81 (1992).
[13] S. Hong, E. Kim, D-.W. Kim, T-.H. Sung, and K. No, J. Non-Cryst. Solids **221**, 245 (1997).
[14] G. P. Schwartz, M. S. Hybertson, J. Bevk, R. G. Nuzzo, J. P. Mannaerts, and G. J. Gualtieri, Phys. Rev. B **39**, 1235 (1989).
[15] S. L. Chuang, *Physics of Optoelectronic Devices* (Wiley, New York, 1995).
[16] J. P. Landesman, J. C. Garcia, J. Massies, P. Maurel, G. Jezequel, J. P. Hirtz, and P. Alnot, Appl. Phys. Lett. **60**, 1241 (1992).
[17] S. Uhlemann and H. Rose, Ultramicroscopy **63**, 161 (1996).
[18] A. Kay, E. Arenholz, S. Mun, F. J. Garcia de Abajo, C. S. Fadley, R. Denecke, Z. Hussain, and M. A. Van Hove, Science **281**, 679 (1998).
[19] E. Arenholtz and C. S. Fadley (private communication).
[20] Y. Gao and S. A. Chambers, J. Cryst. Growth **174**, 446 (1997).